Chapter 2

Experimental Setup

The experimental setup used for the infrared experiments presented in this thesis is based on the instrument constructed by K. R. Asmis[46] and described in the diploma theses of Gabriele Santambrogio,[47] C. Cibrián Uhalte[48] and Oliver Gause.[49] Since then, the equipment was continuously improved and these improvements will be described in this chapter as well. First, the ion sources will be presented followed by the ion guiding tandem mass spectrometer. Furthermore, the infrared free electron laser FELIX will be described. The chapter ends with the description of the measurement procedure of the infrared experiments.

2.1   Ion Sources

For the production of the ions studied in this thesis three different ion sources were used. The *electro-spray source* produces gas phase ions from solution and it is a continuous source. The *laser vaporization source* was used to produce gas phase ions form the solid phase. The third ion source is the *electron impact source* which may run either continuously or in pulse mode and was used in the experiments presented in this thesis for the generation of ions from gas phase neutral molecules.

2.1.1   Electro-Spray Source

The atmospheric pressure electro-spray used for some of the experiments presented in this work is a commercial source produced by Perkin-Elmer Sciex Instruments.

The electro-spray process was first observed and described by John Zeleny in 1914.[50] Later, Malcolm Dole[51] recognized for the first time the possibility of generating gas phase ions by spraying a solution from the tip of an electrically charged needle.

The main interest was to bring biological molecules and polymers without fragmentation from solution to the gas phase. With this technique also small molecules can be transfered to the gas-phase. The general requirement for the electro-spray source to work is that the solute must be soluble in a polar solvent which is volatile and has a low viscosity. The modern electro-spray source combined with a mass spectrometer was developed by John Fenn[52] who received the Nobel Prize in 2002 for the development of methods for identification and structure analyses of biological molecules.
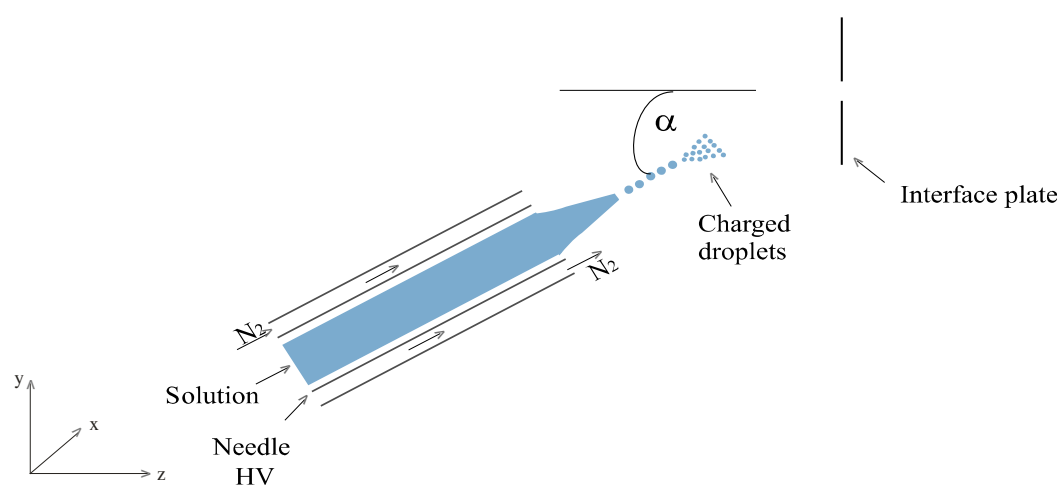

Figure 2.1: Schematic of the electro-spray technique. The solution is passed through a highly charged needle. The formed liquid droplets are accelerated to the interface plate. Flying to the plate, the droplets shrink due to evaporation of neutral solvent molecules. The evaporation of the solvent molecules is facilitated when a nebulizer gas is used, typically N_2. At the interface plate, the naked ions pass a 100 μm orifice into vacuum. The needle can be moved in the x, y, and z direction. The spraying angle α can be modified as well.

Figure 2.1 shows the mechanism of the electro-spray process. A solution, containing the solute and the solvent, with a concentration of less than 10^{-3} M, is pumped by a syringe driver into a capillary tube (0.1 mm) which ends with a highly charged needle ($-4\cdots+6\ kV$). The needle can be moved in the x, y and z direction. The angle α under which spraying of the liquid occurs can also be modified. As the liquid exits the needle (flow rate typically lower than 10 $\mu l/min$) it forms a jet of highly charged droplets with a diameter of less than 10 μm. Strong repulsion electrostatic forces between the charged droplets limit aggregation.

Flying to the interface plate ($\pm 700\ V$), neutral solvent molecules evaporate. A nebulizer gas (N_2) facilitates the formation of small droplets. As the droplet size

decreases, the charge density at the surface increases until it reaches the Rayleigh limit.[53] At this size, due to the repulsion of similar charges, the droplets explode (Coulomb explosion), forming a mist of smaller charged droplets.

For the release of the ions from the small droplets to the gas-phase, two mechanism were proposed. One of the mechanisms, referred to as the *Charged Residual Model (CRM)* was proposed by M. Dole[51] and considers that the Coulomb explosion process is repeated until the naked ions remain. This mechanism implies the formation of very small droplets containing only one ion. The second model, referred to as the *Ion Evaporation Mechanism (IEM)* was proposed by Iribarne and Thomson.[54] They assumed that before the droplets g small enough to contain only one solute molecule, the field strength at the droplet surface becomes intense due to the decrease of the droplet size. If there are enough excess ions, a critical field is reached at which the ions are evaporated into the ambient gas.[52] Recent calculation performed on the hydronium and the diglycine ions support the ion evaporation mechanism.[55]
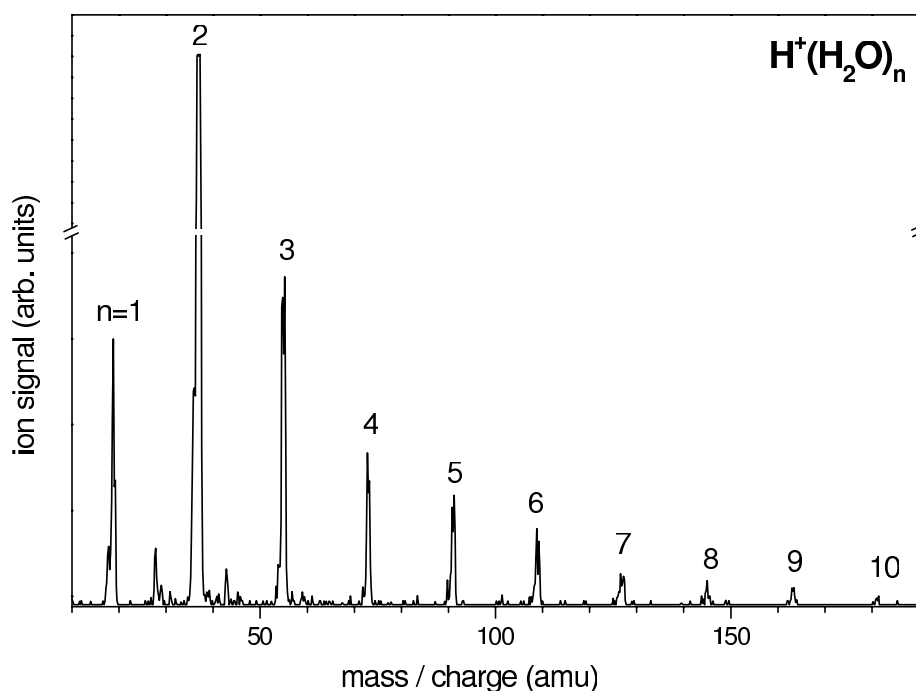
Figure 2.2: Mass spectrum of $H^+(H_2O)_n$ cations generated with the electro-spray source. The voltage on the needle was $+5\ kV$ and the flow rate of the water was $6\ \mu l/min$.

The naked gas phase ions pass a $100\ \mu m$ diameter orifice ($\pm\ 60\ V$) and undergo a free jet expansion into vacuum. Spraying off angle has the advantage that the

neutral molecules and impurities do not enter the vacuum system and the orifice at the interface plate does not clog. In this work, this source was used for generating protonated water dimer cations. A typical mass spectrum of water cations is shown in Figure 2.2.

2.1.2   Laser Vaporization Source

The home-built laser vaporization source was used to produce vanadium oxide cluster ions. A broad spectrum of cations as well as anions can be obtained by this method.

The source is operated with 532 nm radiation, produced by second harmonic generation (SHG) of the fundamental wavelength from a Nd:YAG laser. The laser power is approximately 10 mJ with a pulse duration of 8 ns. The Nd:YAG laser runs with a repetition rate of 20 Hz. The laser radiation is focused by a plan-convex lens with f=150 mm on a vanadium rod (Alfa Aesar 99.5 % purity). In order to avoid the formation of a hole in the target, the rod is rotated and translated by an assembly consisting of a threaded screw which is rotated by a stepping motor placed outside of the vacuum chamber. The leading part of the laser pulse evaporates the metal forming vanadium vapor. The trailing part of the pulse ionizes the vapor creating a plasma.[56] A buffer gas is pulsed normal to the interaction region of the laser with the vanadium rod. For the production of vanadium oxides a mixture of helium and oxygen was used as buffer gas, which is pulsed in by a General Valve (150 μm nozzle) running at 20 Hz. In the vaporization region a broad distribution of clusters is formed containing neutral as well as charged species. Collisions with the buffer gas atoms lead to a thermalization of the clusters to the temperature of the source walls. Larger vanadium oxide cluster ions are produced by nucleation processes. The pressure of the buffer gas and the time delay between the laser pulses and the gas pulses are important for the size distribution of the formed clusters. These two parameters are optimized by monitoring the ion cluster intensity. Figure 2.3 shows a typical mass spectrum of vanadium oxide cations recorded up to a mass of 800 amu. As observed from Figure 2.3, a broad distribution of masses can be produced.
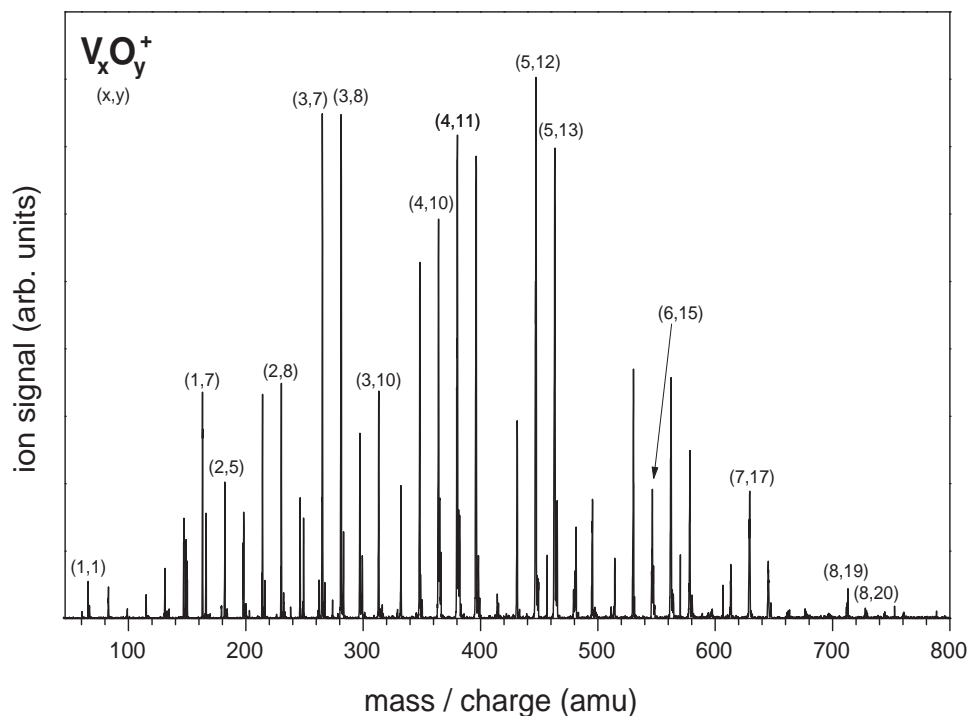
Figure 2.3: Typical mass spectrum of vanadium oxide cations ($V_xO_y^+$) produced with the laser vaporization source. The laser was running at 532 nm with a pulse energy of 10 mJ. The carrier gas consisted of 1% O_2 in He.

2.1.3   Electron Impact Source

Anions as well as cations can be produced with the electron impact source. The electron impact source consists of a molecular beam apparatus and an electron gun. The molecular beam is produced either by a pulsed source or a continuous source. The pulsed source contains a general valve (150 μm diameter nozzle) which was operated at 20 and 100 Hz. The gas expansion contains a certain amount of the gas (HBr or DBr) seeded in helium or argon. The optimal concentration and the backing pressure depend on the system of interest. The continuous source consists of a tube with 10 mm diameter which ends with an exchangeable plate having a small orifice in the middle. The orifice diameter can be varied between 10 μm to 100 μm. The holes were drilled by the *Laser- und Medizin-Technologie GmbH Berlin* company. The molecular beam is intersected with a beam of electrons from a 300 μA, 1 keV electron gun received form D. Neumark, University of California, Berkley, U.S.A (see
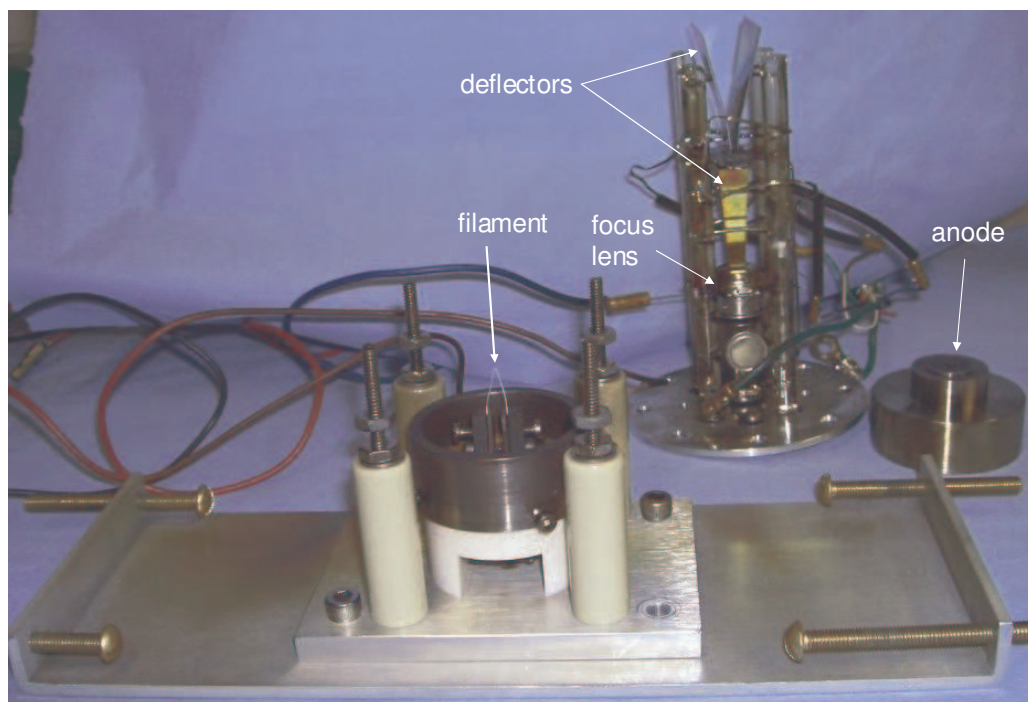
Figure 2.4: A photograph of the electron gun received form D. Neumark, University of California, Berkley, U.S.A.

Figure 2.4). The electron gun consists of a thorium-coated iridium filament (cathode) which is heated until the energy of the electrons in the filament is high enough to exit the surface. The electrons are accelerated towards the anode and pass through a hole placed in its center. A focusing lens is used to collimate the electron beam. Voltages applied to two deflector plates are used to control the beam position in the x and y direction. The potentials for the electron gun were provided by a power supply built at the electronic workshop of the Freie Universität Berlin (see Appendix A).

In this thesis, the source was used for the generation of negative ions, which are produced in the electron beam-free jet interaction region. Anions can be produced by electron attachment of low energy electrons, where three-body stabilization is important:

$$XY + e^- + M \rightarrow XY^- + M$$

where M is usually a rare gas atom. A second possibility to produce anions by electron impact is represented by the dissociative attachment process:

$$XY + e^- \rightarrow (XY^-)^* \rightarrow X^- + Y$$
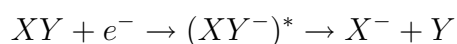
Efficient dissociative attachment requires electrons with low energies ($< 20\ eV$).[57]

As a consequence, for the mechanism of anion formation in the case of high energy electron beams of 1 keV, as is the case here, secondary electrons with low energies play an important role. Secondary electrons are produced through collisions of the high energy electrons with the buffer gas:

$$e^-(1keV) + X \rightarrow X^+ + e^-(slow) + e^-(fast)$$
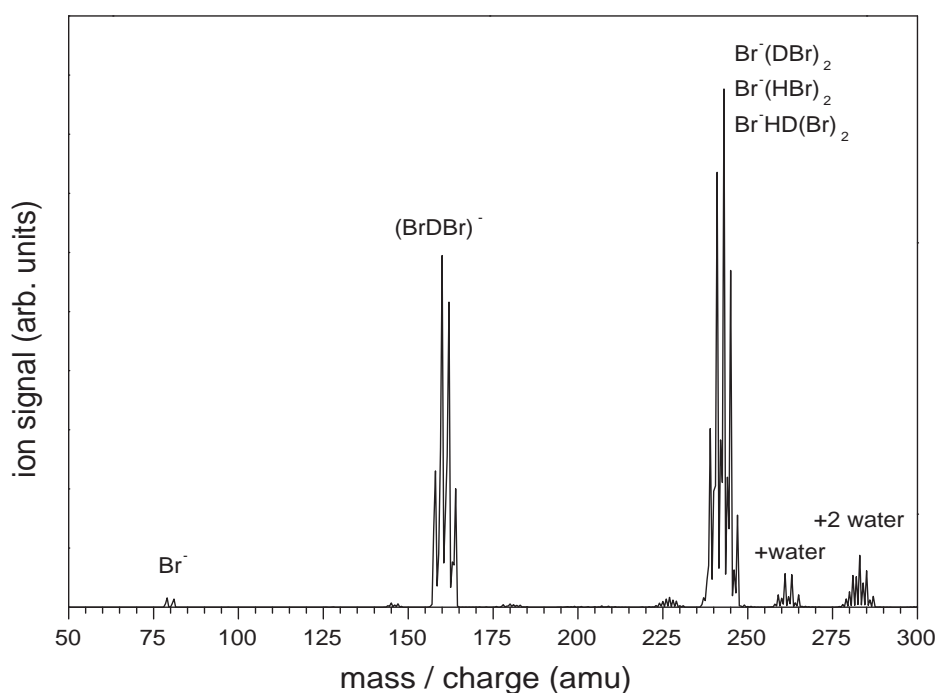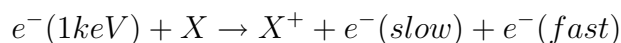
Figure 2.5: Mass spectrum of $Br(D(H)Br)_n^-$ anions produced with the electron impact source. A gas mixture of 0.5 % DBr in Ar was pulsed in the ion source chamber by a general valve running at 100 Hz and with an nozzle of 150 μm diameter. The molecular beam was intersected by a beam of electrons producing anions by dissociative electron attachment. The assignment of the peaks is shown in the mass spectrum. The presence of a low amount of hydrogen in deuterium is evidenced by the formation of $Br^-(HBr)_n$ and $Br^-HD(Br)_2$.

Alexander *et al.*[58] studied the dependence of the distance of the electron beam from the nozzle of the molecular beam apparatus in the mass distribution of the complexes. Large anions are preferentially formed close to the nozzle, where the three-body collisions required for clustering are favored, whereas small anions are formed further in the expansion.

The electron impact source works well with gaseous chemicals and was used for the formation of hydrogen dihalides and solvated hydroxyl anions. Typical mass spectra are shown in Figure 2.5 and 2.6.
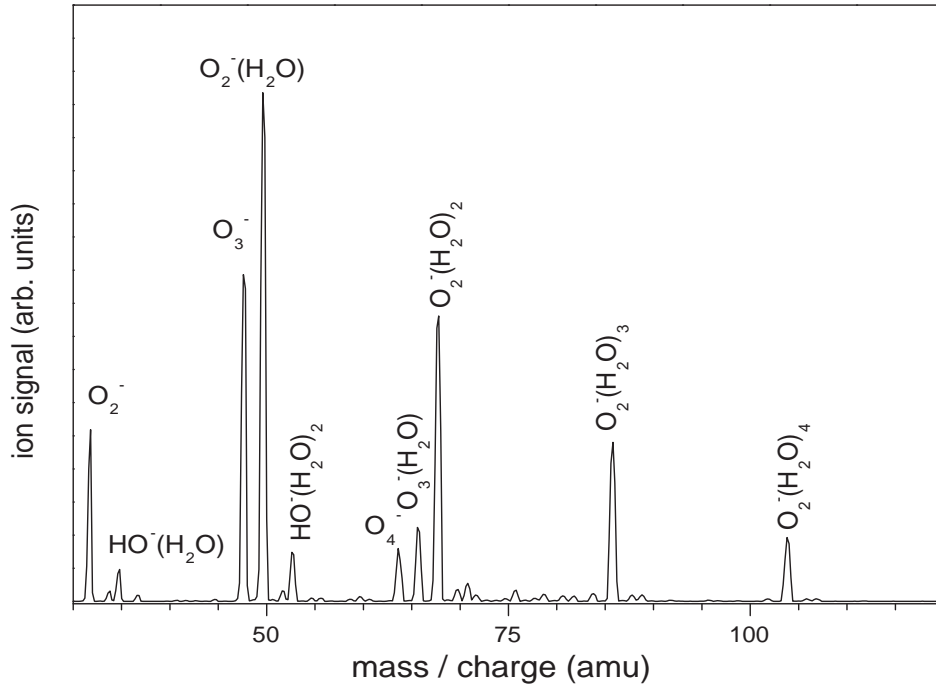
Figure 2.6: Mass spectrum of solvated hydroxyl anions generated with the electron impact source. A mixture of 10 % O_2 in He was passed over a small amount of water and transfered to vacuum through a 0.31 μm diameter nozzle. The molecular beam was intersected by a beam of electrons producing anions by dissociative electron attachment. The assignment of the peaks is shown in the mass spectrum. Intense peaks due to the formation of O_n^- and $O_2^-(H_2O)_n$ molecules are observed.

2.2   The Ion Guiding Tandem Mass Spectrometer

The apparatus used for the experiments presented in this work consists of two vacuum parts, the ion source and the main chambers. The two parts are separated by a gate valve (GV). The gate valve is closed when the ion source needs to be changed or cleaned. In this way, only the source chamber needs to be vented and the rest of the apparatus remains under vacuum. The main chamber is placed on a movable table which enables the joining and the separation of the two vacuum parts.

A schematic of the apparatus is shown in Figure 2.7. The ions formed by using one of the methods described in the previous section pass the source into the next vacuum chamber via a skimmer (S) with an opening of 2 mm diameter. After passing the skimmer, the ions are focused by an electrostatic lens into a home-built radio frequency ion guiding decapole (Q_0). The decapole can be filled with gas, generally helium or argon. Due to the collisions with the rare gas atoms, the ions will thermalize
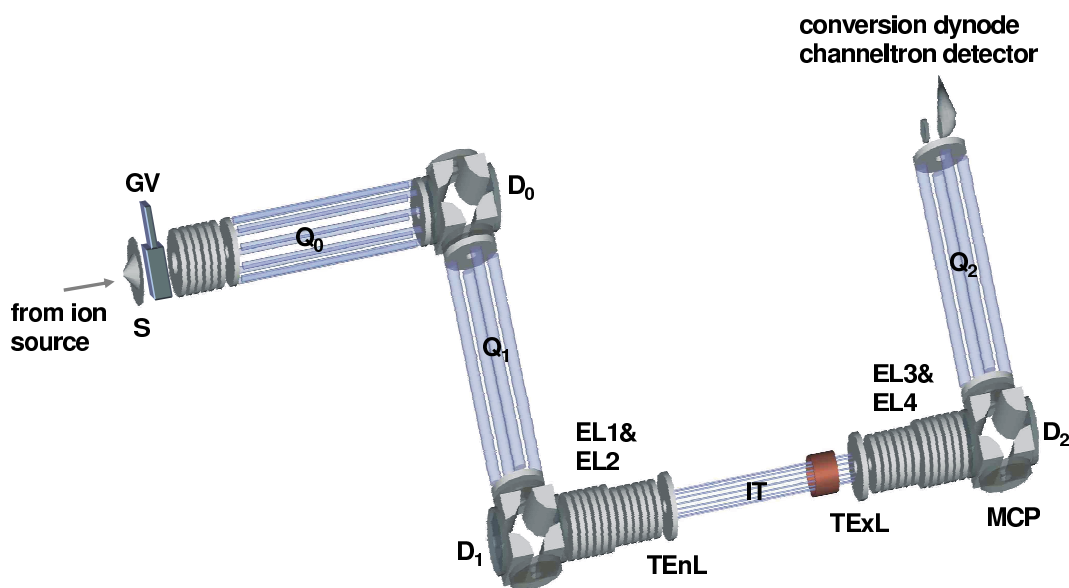
Figure 2.7: The ion guiding tandem mass spectrometer. S - skimmer, GV - gate valve, $Q0$ - ion guiding decapole, $D0$, $D1$, $D2$ - 90° quadrupole ion deflectors, $Q1$, $Q2$ - RF quadrupole mass filter, $EL1$, $EL2$, $EL3$, $EL4$ - einzel lenses, IT - He filled, temperature adjustable RF hexadecapole ion trap, $TEnL$, $TExL$ - trap entrance and exit electrostatic lenses, MCP - multichannel plate detector.

and the molecular beam will be collimated by reducing its kinetic energy distribution. When weakly bound complexes (such as $BrHBr^- \cdot Ar$) are generated in the source, the collisions with the He or Ar atoms lead to a partial fragmentation of the weakly bonded ions, process referred to as collision induced dissociation (CID). After the thermalization process, the ion trajectories are bent by a 90° quadrupole deflector ($D0$) and the ions are guided into the first quadrupole mass filter ($Q1$). Here the voltages related to the mass to charge ratio, can be set so that only the ions of interest will have stable trajectories and pass the filter. For ions with low dissociation energies, the mass spectrometer filters the unwanted background formed by CID in the decapole. After another 90° turn by a second deflector ($D1$) a system of einzel lenses $EL1$ and $EL2$ focuses the ions into a home-built hexadecapole radio frequency ion trap (IT). Here, the laser experiments are performed. A detailed description of the function of the decapole and of the ion trap is discussed in the following subsection. The trajectories of the products (e.g., dissociation products) are further bent by the third deflector ($D2$) and focused by another set of einzel lenses $EL3$ and $EL4$ into the second mass filter ($Q3$). The products are mass selected and detected by a dynode conversion channeltron detector. A multi-channel plate (MCP) detector can also be used for detecting the ions. This can be placed after each deflection facilitating the

adjustment of the potentials so that the ions reach the channeltron detector.

The apparatus operates under vacuum conditions. Pressures up to $10^{-8}-10^{-9}$ $mbar$ can be achieved in non-operating conditions. The main vacuum chamber is pumped by four 520 l/s turbo-molecular pumps and the ion source chamber is pumped by a larger turbo-molecular pump (1600 l/s). When the experiments are running the ion source chamber reaches pressures of 10^{-3} $mbar$. In the region of the $Q0$ decapole, the pressure reaches approximately 10^{-4} $mbar$ and depends on the amount of the He or Ar gas necessary for the thermalization. The $Q1$ and the ion trap regions run usually at 10^{-6} $mbar$ and the last mass filter region has a pressure of 10^{-7} $mbar$.

In order to control the potentials on different parts of the apparatus, a LabView program was developed in our group. This program controls the guiding of the ions, the mass selection as well as the trapping and the measurement process.

2.2.1 The Radio Frequency (RF) Guiding Decapole and the Hexadecapole Ion Trap

The RF Guiding Decapole

The RF guiding decapole (ten rods) is used not only for guiding but also for the thermalizaion of the ions. The electrodes are placed on a circle with a diameter of 25 mm in a 52 mm diameter cylindrical housing with a length of 230 mm. The diameter of the rods is 5 mm. An RF potential with a frequency of 1.2 MHz is applied to the rods. Thermalization of the ions is achieved by collisions with He or Ar atoms. Due to the collisions with the buffer gas atoms, the ions are thermalized to the temperature of the buffer gas. The temperature of the ions achieved after a certain number of collisions with the buffer gas is given by the following expression:[59]

$$T_c(m) = (T_c(0) - T_g)(1 - \frac{k}{3nk_B})^m + T_g \qquad (2.1)$$

where $T_c(m)$ represents the temperature of the ions after m collisions, $T_c(0)$ is the initial temperature of the ions before the collisions, T_g denoted the buffer gas temperature, n is the number of the atoms in the ion and k represents an energy exchange parameter. k depends on the atomic mass of the buffer gas, the atomic mass of the cluster and the interaction strength.[59]

Simulations performed by Carlos Cibrián Uhalte[48] with the SIMION 7.0 program on this decapole have demonstrated that approximately 1200 collisions are necessary to thermalize the ions to the rare gas temperature. These simulations predict that

the thermalization process for an ion with a mass of 164 *amu* and *He* pressure of 0.0133 *mbar* at a temperature of 100 *K* takes places in less than 10 *ms*.
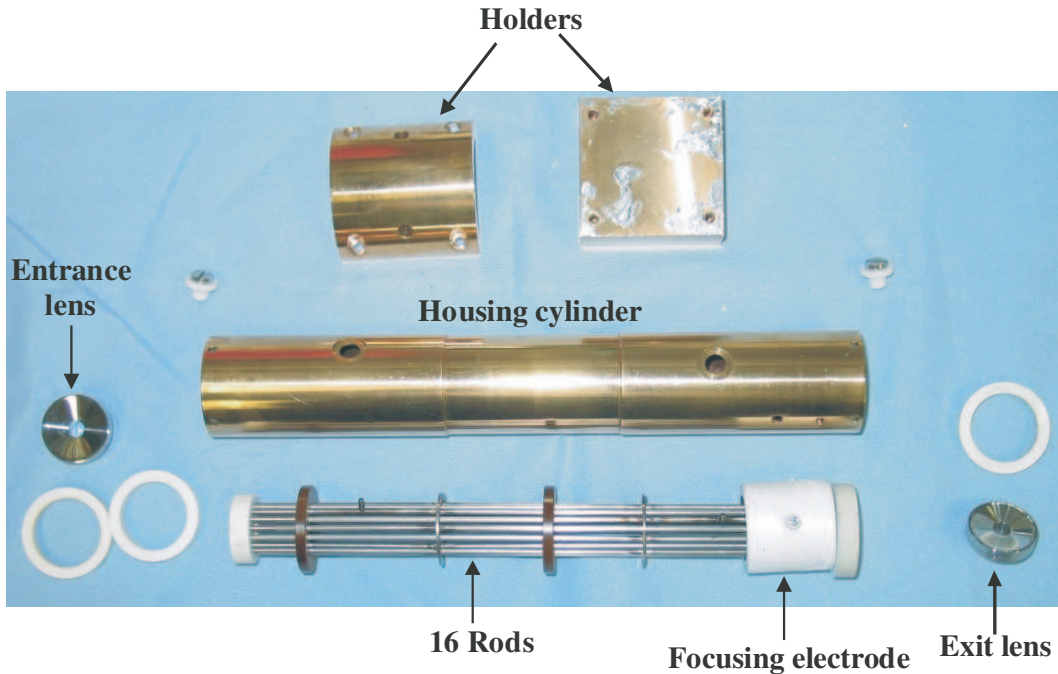

Figure 2.8: The hexadecapole ion trap. The photograph shows the entrance ($TEnL$) and the exit lenses ($TExL$), the 16 metallic rods, a focusing electrode and the gold plated copper housing cylinder. In the upper part of the photograph the holder which connects the trap to the cryostat head is shown.

Hexadecapole ion trap

Trapping of the ions becomes necessary, due to the low ion density in the gas phase. By trapping, the ion density can be increased up to the space charge limit ($\approx 10^8 \ ions/cm^3$). Trapping is performed in a hexadecapole (16 rods) which is similarly constructed as the RF guiding decapole. Here, the laser experiments are performed. The laser radiation enters the trap collinearly with the ions through a window placed at the end of the trap arm. On the other side of the arm a second window is placed. The bent form of the apparatus facilitates the alignment of the laser through the trap and interactions of the laser with the ions in the mass filters is avoided. In all experiments presented in this thesis, the laser was aligned slightly off-axis. The angle under which the laser passes the trap has a maximal value allowed by the diameter of the entrance ($TEnL$) and exit lenses ($TExL$).

A photograph of the hexadecapole ion trap is shown in Figure 2.8. The trap

consists of two electrostatic lenses, an entrance and an exit lens ($TEnL$ and $TExL$ in Figure 2.7) and sixteen metal electrodes. The electrostatic lenses have an inside diameter of 6 mm and the rods are 2 mm in diameter and 20 cm in length. The total length of the trap measures 22 cm. In some experiments a 3 cm long focusing electrode is used. Its function is to create a potential minimum in order to accumulate the ions in this region. When the electrode is used, the laser is also focused to the region of
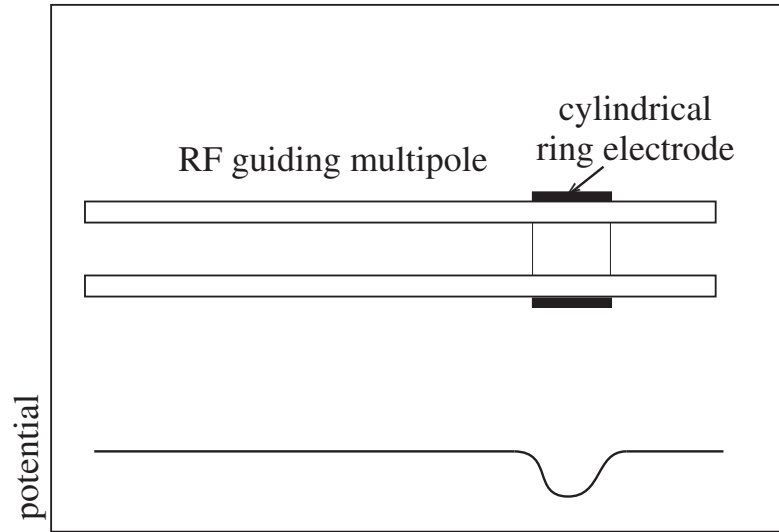
Figure 2.9: Schematics of a multipole with a cylinder ring electrode. The lower panel shows a schematic representation of the potential along the axis of the system. The electrode lowers slightly the potential. Typical values are of a few millivolts per volt applied to the ring.[60]

the focusing electrode. The rods, the lenses and the focusing electrode together with some macor isolating parts are fixed in a gold plated copper cylindrical housing. The housing is fixed to the cooling head of a two stage cryostat by a holder plate. The cryostat cools the hexadecapole to temperatures below 20 K. Trap temperatures as low as 14 K have been achieved when a home-built gold plated copper heat shield was used. The shield is cooled by the first stage of the same cryostat but another cool finger to approximately 77 K. In this way the heat shield protects the trap from the warmer environment. Temperature measurements are made at the middle and at the end of the trap; the temperature difference is about 2 K. The temperature of the trap can be adjusted between 14 K and 350 K. For this purpose, a heater is fixed in the holder plate. For temperature measurements and heating, a LakeShore temperature controller Model 331 is used. Due to the low temperatures used in all the experiments, high purity gases are required. To avoid unwanted impurities to freeze on the electrodes and to increase the purity of the gases introduced into the trap, the

stainless steel tubes transporting the gas from the gas bottle to the trap are passed through a Dewar container filled with liquid nitrogen. Gases with freezing points above 77 K will freeze on the tube walls and will not enter the trap. The pressure at the middle of the trap is measured by a manometer from MKS, Model Baratron 627B. Baratrons are widely used for accurate measurements of low pressures, between 0.02 and 1000 $mbar$. The pressure measurement is independent of the type of the measured gas sample. The pressure measurement is based on the deformation of a metal membrane which is kept at a temperature of 318 K. Since the temperature of the gas in the trap is different as the one of the membrane, the measured pressure must be corrected for thermal transpiration:

$$p_{real} = p_{meas}\sqrt{\frac{T_{trap}}{T_{meas}}} \tag{2.2}$$

where p_{real} denotes the corrected value of the pressure, p_{meas} is the measured value of the pressure, T_{trap} represents the hexadecapole ion trap temperature and T_{meas} is the calibration temperature of the Baratron (318 K).[61]

The trapping mechanism is shown in Figure 2.10. The trap is filled with He as buffer gas. Filling the ion trap with He is essential for thermalization and trapping.[60,62] The trapping process starts with opening the entrance lens ($TEnL$). Ideally, the value of the potential on this lens is chosen so that the ions have a minimal amount of kinetic energy necessary just to overcome the potential barrier of the electrostatic lens. After the ions enter the trap, they collide with the He atoms in the trap. Through collisions with the He buffer gas (in most of the experiments the He pressure was approximately 0.015 $mbar$), the ions lose energy, so that their kinetic energy is not sufficient to allow them to pass back over the entrance lens potential. The filling time for the experiments presented in this work was between 150 ms and 1000 ms, depending on the efficiency of the ion production. This time is sufficient for the thermalization of the ions as showed by the simulations performed on the decapole. Depending on the mass of the ions, thermalization occurs in few ms. During the filling process the exit electrostatic lens ($TExL$) remains closed. This means that the value of the potential creates a barrier which the ions cannot overcome. In this way, the ions can be trapped for up to few seconds.
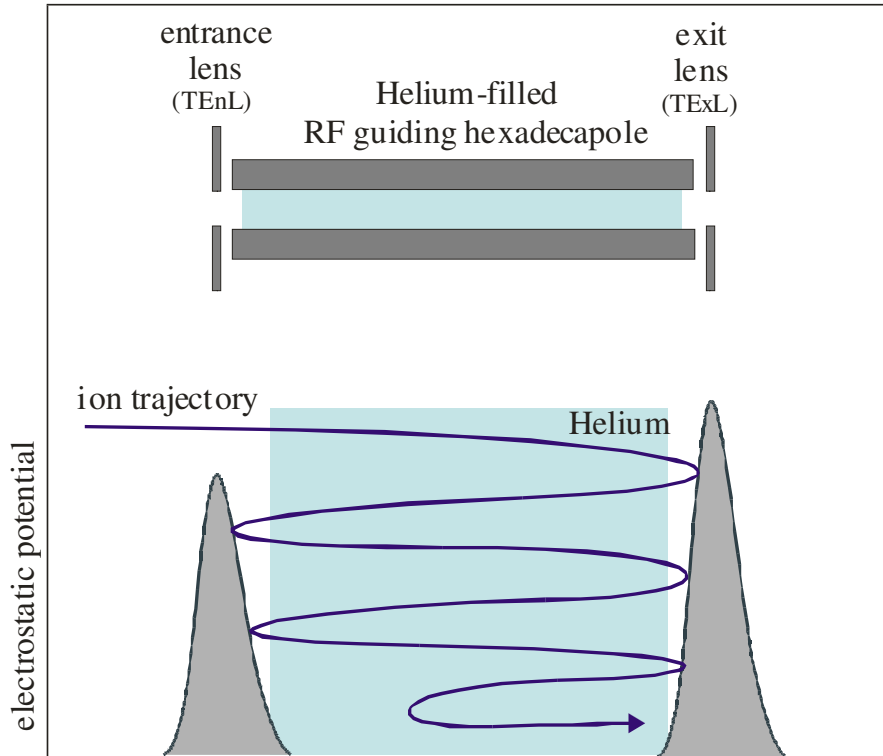
Figure 2.10: The trapping process. The upper part of the figure shows the ion trap filled with He buffer gas and the entrance ($TEnL$) and exit ($TExL$) electrostatic lenses. In the lower part of the figure, the trapping procedure is presented. The ion trajectory shows how the ions lose kinetic energy during the collision with the He gas atoms.

2.3 The Free Electron Laser for Infrared eXperiments (FELIX)

The infrared radiation used in the experiments is produced by the Free Electron Laser for Infrared eXperiments FELIX, situated at the Fundamenteel Onderzoek der Materie (FOM), Institute for Plasma Physics, Rijnhuizen, the Netherlands.

2.3.1 Radiation characteristics and FELIX design

In a free electron laser, radiation is produced by free electrons which move at relativistic speeds under the influence of a magnetic field with periodically changing polarity. Figure 2.11 shows a schematic of a free electron laser.

Electrons, generated by an electron gun, are accelerated at relativistic energies in an electron accelerator. The produced relativistic beam of electrons is injected into a magnetic field structure referred to as undulator. The undulator consists of a series
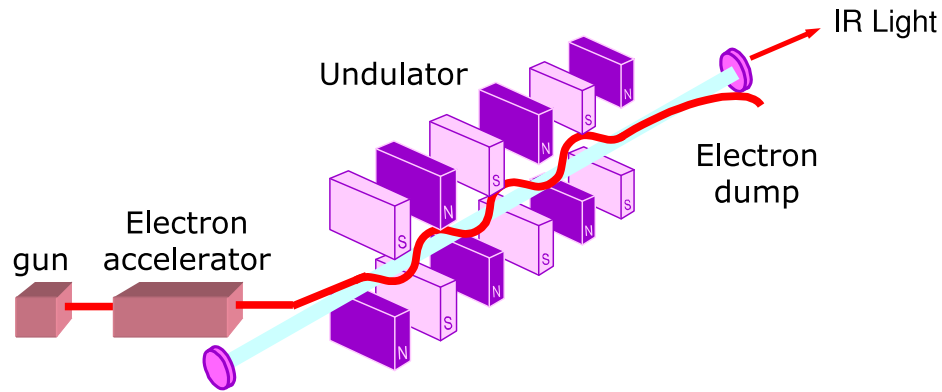
Figure 2.11: Schematic of a free electron laser consisting of an electron gun, an accelerator and a magnetic field structure (undulator), which is placed in a resonator cavity. The undulator consists of permanent magnets with changing polarity. The red line shows the trajectory of the electrons in the cavity. The radiation is represented by the light blue colored thick line, between the two cavity mirrors. The radiation is coupled out through a hole in the center of the cavity mirror placed at one end of the resonator. (Figure received from the FOM Institute, Rijnhuizen, the Netherlands.)

of equally spaced permanent magnets. The FELIX undulator consists of thirty-eight pairs of samarium-cobalt permanent magnets, with 65 mm period length.[63] The undulator is placed inside an optical resonator. Two gold plated copper mirrors, one attached to a precision translation stage, define the resonator cavity. The resonator has a length of 6 m (see Figure 2.12).

Entering the undulator, the electrons experience a magnetic field which is perpendicular to their trajectories and changes polarity periodically. This induces a "wiggling" motion of the electrons as they traverse the undulator. This motion is similar to the motion of the electrons in a dipole antenna, resulting in emission of radiation with the frequency equal to the oscillation frequency. The oscillation frequency is given by the ratio of the velocity of the electrons to the length of one period of the path traveled by the electrons.[64] Due to this transverse motion induced by the magnetic field, the period of the path of the electrons is larger than the period of the undulator λ_u. The difference in path length between electrons and radiation is $(1 + K^2)$.[64,65] K is a dimensionless parameter with a value close to 1 and is a measure of the magnetic field.

The emitted radiation appears in the laboratory frame Doppler shifted, the wavelength of the forward emitted radiation being reduced by a factor on the order of γ^2 relative to the length of the undulator period. The Lorentz factor γ is a measure of the total electron energy. As a consequence of the Doppler effect, the energy of the radiation emitted by the relativistic electrons is concentrated in a narrow cone in the forward direction. At FELIX, γ can be varied between 20 and 100. Considering the 65 mm period of the undulator, the radiation is emitted in the infrared wavelength range (see equation (2.3)). This radiation is referred to as spontaneous emission.[64,65]

$$\lambda_s = \frac{\lambda_u(1 + K^2)}{2\gamma^2} \tag{2.3}$$

The electrons coming from the accelerator are typically spread out over an interval much larger than the radiation wavelength. Thus, the electrons emit incoherently and the spontaneously emitted radiation is very weak. Through successive round trips in the undulator, this weak radiation can be amplified by fresh electrons, until saturation sets in.
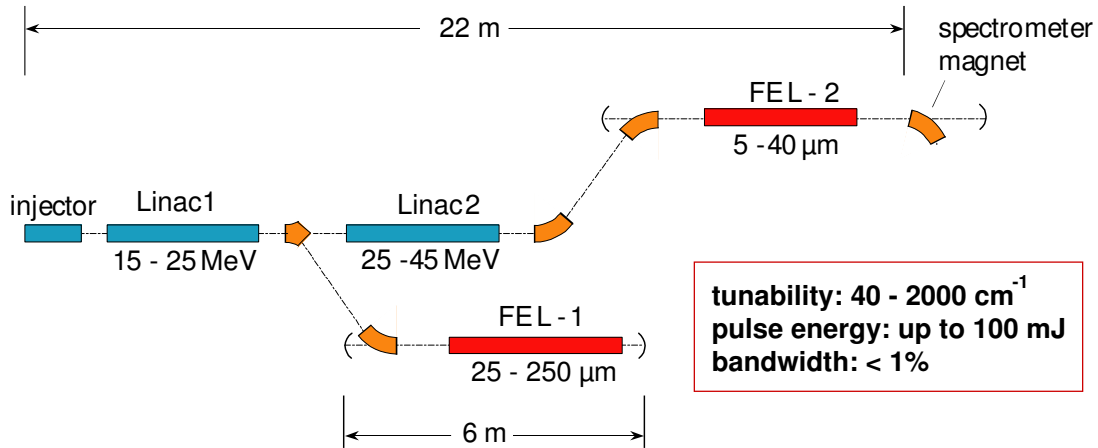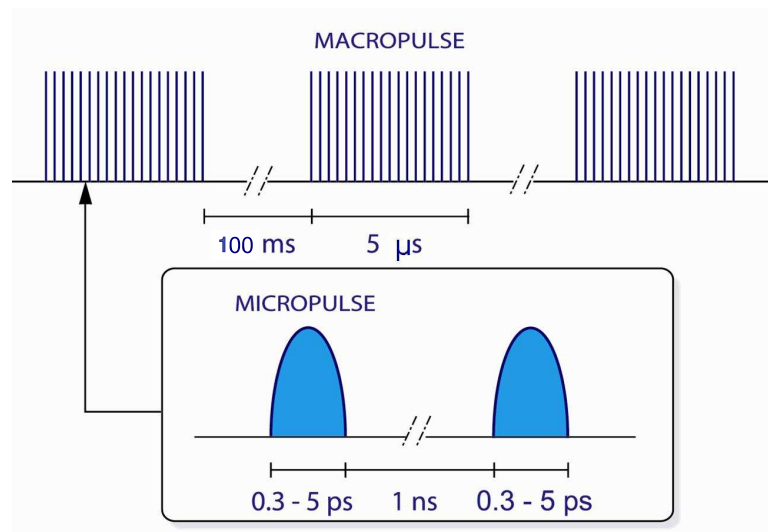

Figure 2.12: Schematic of the Free Electron Laser for Infrared eXperiments (FELIX) situated at the FOM Institute for Plasmaphysics, Rijnhuizen, the Netherlands. Linac 1 and Linac 2 represent two radio frequency linear accelerators which accelerate electrons to relativistic energies. Each Linac is followed by one FEL, which consists of an undulator placed in a 6 m long resonator cavity. The inset shows few characteristics of the FELIX radiation. (Figure received from the FOM Institute, Rijnhuizen, the Netherlands.)

Radiation amplification is achieved by the interaction between the electrons and the spontaneous emitted radiation which causes microbunching of the electron beam

leading to coherent emission. Considering first only one electron entering the undulator at resonance energy[a], interaction between this electron and the existing spontaneous radiation leads to an energy transfer from the kinetic energy of the electron to the radiation or the opposite way. This results in an acceleration or a deceleration of the electron, depending on the relative phases of the electron oscillations and of the radiative field. In a beam, the electrons are uniformly distributed over all phases and averaging over all electrons, at resonance, a zero net gain is obtained. Due to the phase dependent energy transfer and associated velocity modulation, a density modulation on the wavelength scale (micro-bunching) will develop along the undulator.[65] At resonant energy micro-bunching is around a phase corresponding to zero net gain. When the electrons are introduced in the undulator at an energy slightly above the resonant value, bunching around a phase corresponding to positive net gain is obtained. Saturation sets in at a power level that is typically 10^6 to 10^8 times higher than that of the spontaneous emission.


Figure 2.13: The pulse structure of the free electron laser FELIX. The macropulses are 5 μs long spaced by 100 ms. Each macropulse contains a few thousand micropulses with 0.3 to 5 ps duration, spaced by 1 ns. (Figure received from the FOM Institute, Rijnhuizen, the Netherlands.)

The time structure of the radiation mimics the time structure of the electron beam. The FELIX pulse structure consists of macropulses with a duration up to 10

---

[a]The radiation is in resonance with the electron if the radiation advances by an integer number (= harmonic number) of radiation wavelengths relative to the electron, for each oscillation of the electron in the undulator field.

μs and a repetition rate up to 10 Hz. For the experiments presented in this thesis, the macropulse duration was 5 to 7 μs at a repetition rate of 5 Hz. Each macropulse consists of a few thousand micropulses with variable pulse length ranging from 0.3 to 5 ps typically spaced by 1 ns (see Figure 2.13).

For the experiments presented in this thesis, the tunability and the high intensity of the FELIX pulses are very important. The radiation wavelength is determined by the electron beam energy and the periodicity and the strength of the magnetic field in the undulator. At FELIX, the wavelength can be tuned between 5 to 250 μm. Since the undulator period λ_u is fixed by construction, the wavelength can be varied by increasing the amplitude of the magnetic field K. This is achieved by adjusting the gap between the pairs of the magnets by means of stepper motors. The wavelength tuning for a given setting of the beam energy is limited to a factor two to four in the wavelength.[64] For the experiments presented in this work, the used wavelength range was between 5 to 20 μm. This range can be scanned within few minutes.
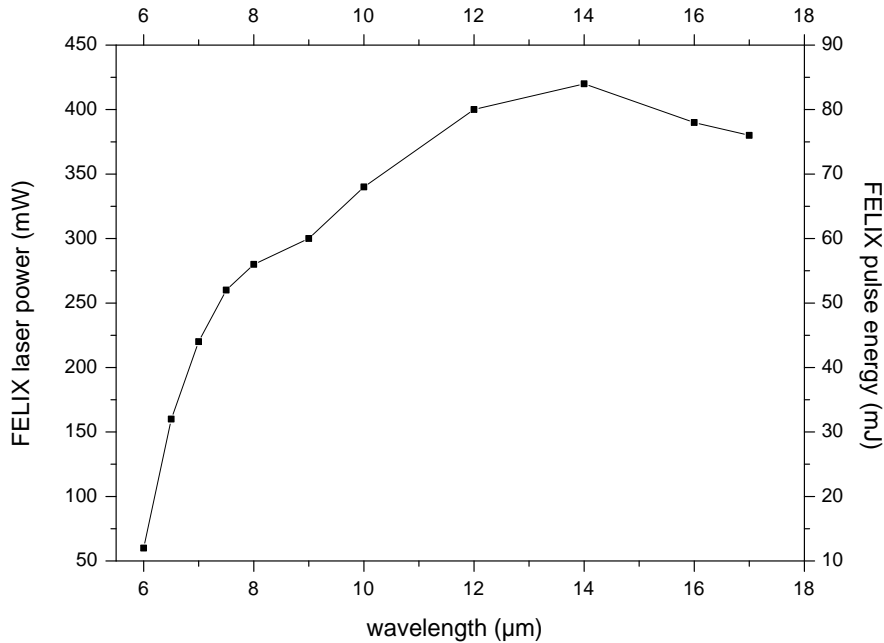
Figure 2.14: Typical evolution of the FELIX laser power over the scanning range used in the experiments presented in this thesis. The right axes shows the macropulse energy at a repetition rate of 5 Hz.

FELIX emits intense radiation, with pulse energies up to 100 mJ. FELIX is adjusted such that the pulse energy changes as little as possible over the scanning range. A typical evolution of the laser power is shown in Figure 2.14. The bandwidth

of the laser is transform limited[b] and can be varied between 0.4% and 7% full width at half maximum (FWHM) of the central wavelength. For the experiments presented in this thesis, the bandwidth was usually chosen to be on the order of 0.5% to 1% FWHM of the central frequency.

2.4 The Measurement Procedure

The measurement procedure is set as follows (see Figure 2.15): The opening of the entrance lens ($TEnL$) is triggered by a TTL signal few μs after the FELIX macropulse. The exit lens ($TExL$) remains closed. The hexadecapole ion trap is filled for typically 150 ms. After filling the trap, the entrance lens ($TEnL$) is closed. The laser macropulse enters the trap and eventually photodissociation occurs. The opening of the exit lens ($TExL$) is again triggered by a TTL signal from FELIX. The ion extraction follows during few ms, typically less than 40 ms. If the focus electrode is used, the ions can be extracted faster from the trap.

Depending on the signal intensity the process is repeated for 5 to 20 fill/extraction cycles for each fragment. The parent ion is always measured at the beginning and at the end of each wavelength step. For longer filling times the measurement procedure is identical but a larger number of macropulses will interact with the ions. A typical overview spectrum is measured with a wavelength step of 0.1 μm. Higher resolution spectra with a step of 0.01-0.04 μm are recorded over narrower ranges where infrared activity is observed. After each wavelength step the trap is completely emptied.

The infrared laser is focused in the trap by a 479 mm KBr lens. For some experiments also $ZnSe$ windows and lenses were used. The $ZnSe$ material has a lower transmission of infrared radiation in the short frequency range. The transmission spectra of the KBr and $ZnSe$ material is shown in Appendix B. The laser is scanned over a wide range of frequencies. When FELIX is in resonance with one of the infrared transitions of the trapped ions, photon absorption and dissociation can occur leading to the production of dissociation fragment ions.

$$XY^{+/-} \overset{h\nu_{IR}}{\rightarrow} (XY^{+/-})^* \rightarrow X^{+/-} + Y; X + Y^{+/-} \tag{2.4}$$
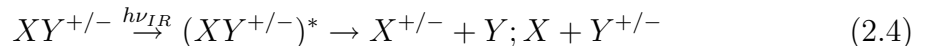
There are two ways of measuring the infrared spectrum:
a) One possibility is the detection of the fragment ion as a function of the laser

---

[b]A pulse is referred to as Fourier transform limited when the equality: $\Delta\nu\Delta t = K$ is satisfied. $\Delta\nu$ is the frequency full width at half maximum, Δt represents the half maximum duration and $K = 0.441$ for Gaussian pulses. The phase variation of a transform limited pulse has a linear time dependence.
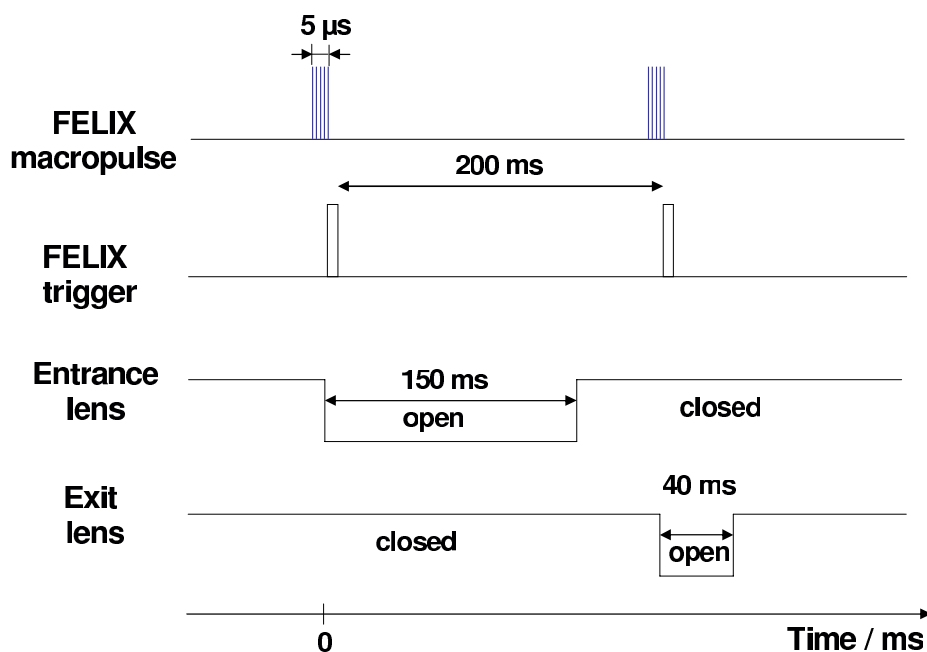
Figure 2.15: Schematics of the measurement procedure. Plotted are the FELIX macropulse and the FELIX trigger which repeat every 200 ms, due to the repetition rate of the laser (5 Hz). In the lower part the entrance ($TEnL$) and the exit lens ($TExL$) voltages are presented.

frequency.

b) The second method is the detection of the depletion of the parent ion signal as a function of the laser frequency.

Oscillations of the parent ion signal due to the instability of the ion source of about 10% from the total ion signal reduce the detection sensitivity of the bands with low intensities. Due to this reason, in some experiments, the first method, which is usually background free, is prefered.